

HIGHER PHOTO SENSITIVITY OF Co-Y-OXIDE NANO STRUCTURE SYNTHESIZED BY HYDROTHERMAL METHOD

S. A. HAMDAN, I. M. ALI

Dept. of Phys., College of science, University of Baghdad

In this work, Co-Y-oxide Nano Structure is successfully synthesized via hydrothermal method. The XRD analysis, SEM analysis, optical, electrical and photo sensing properties have been investigated for Co_3O_4 and Co-Y-oxide thin films. The X-ray diffraction (XRD) analysis reveals that all films are polycrystalline in nature, having cubic structure. The SEM images of thin films clearly indicates that Co_3O_4 possesses nanosphere like structure and flower like for Co-Y-oxide. The optical properties show that the optical energy gap follows allowed direct electronic transition calculated using Tauc equation and it increases for Co-Y-oxide. The photo sensing properties of thin films are investigated as a function of time at different wavelengths to find the sensitivity for these lights. For Co_3O_4 , photo sensitivities are 39.7% and 40% at wavelengths 470nm and 600nm respectively, while for Co-Y-oxide, photo sensitivities are 84% and 111% for these wavelengths. So, higher sensitivity is obtained for Co-Y-oxide with fast rise and fall times less than 1s.

(Received February 7, 2018; Accepted July 21, 2018)

Keywords: Cobalt Oxide, Yttrium, Photo Sensor, Sensitivity, Hydrothermal.

1. Introduction

Cobalt oxide (Co_3O_4) is an important P-type semiconductor with direct optical band gaps at 1.48 and 2.19 eV [1,2]. Among the transition metals oxides, cobalt oxide (Co_3O_4) is a promising material for use as a gas sensor and catalyst in hydrocracking processes of crude fuels, pigment for glasses and Ceramic. Highly dispersed nanostructured spinel cobalt oxide is expected to display better performance in the above mentioned application aspects. Specific morphologies and crystallographic phases of nanostructures materials are responsible for their optical, magnetic and electric properties [3]. In recent years, many efforts have been devoted to the synthesis of Co_3O_4 nanostructures with different morphologies such as nanoparticles, hollow spheres, nanorods, nanoplates, nanowires, nanotubes, nanocubes and nanoporous structures. Among them, Co_3O_4 nanoparticles have been prepared by various physical and chemical techniques such as Combustion method, microwave irradiation, hydrothermal/ solvothermal method, sol-gel process, chemical spray pyrolysis, sonochemical method, polyol method, and so on. Most of these methods need some Special instruments, harsh conditions, and relatively high processing temperature higher than 350°C. In addition, these methods are either time-consuming or require expensive instruments [4]. Hydrothermal synthesis can be defined as a technique that depends on the solubility of minerals in hot environment under high pressure to obtain interested nanostructure where the crystal growth is performed in an instrument consisting of a steel pressure vessel called an autoclave [5].

Photoconductivity (PC) is defined as electrical conductivity resulting from photo-induced electron excitations in which light is absorbed. In semiconductors, photoconductivity arises due to interaction of photons with bound electrons of lattice atoms that leads to photo-generation of electron-hole pairs after absorption of photons which increases carrier density and conductivity of material [6]. PC is an important tool to study the properties of semiconducting materials such as the nature of photo-excitation and recombination processes. The conductivity of material depends upon the carrier density, carrier lifetime and complex process of carrier generation, trapping, and recombination [7]. It is also a function of temperature, applied field, intensity of light and energy

*Corresponding author: suhadah22@gmail.com

of radiation [8]. Extensive study of photoconductivity has been made in nanoparticles, thin film, nanorods, nanowires and mixed lattice [5,9-11], and [12] for different parameters.

This study aims to prepare pure cobalt oxide nanoparticle and cobalt yttrium oxide and study their structural, morphological, optical properties and its applications as a photosensor device.

2. Experimental

Pure cobalt oxide and yttrium cobalt oxide thin films have been prepared by hydrothermal method onto seeded layer. Firstly, to prepare seeded layer, PVA ($C_4H_6O_2$)_n will be used which dissolved in distilled water. The aqueous solutions of cobalt nitrate and Yttrium nitrate with 0.1M are stirred separately on magnetic stirrer for 10 min to prepare the precursors which are the sources of cobalt and yttrium ions. Then, cobalt precursor is added to 1.5 g of PVA at 80 °C for 2h. This solution is irradiated with 2.4 GHz microwave frequency at power 220 W for 10 min then measuring pH for solution and controlled its value to 8 or until changing the color of solution. The resultant solution has been spin coated onto silicon and glass substrates at 1500 rpm for 1min, this step was repeated several times to obtain the desired thickness for seed layer.

The above steps are for preparation of pure seed layer solution, for preparing seed layer solution with Yttrium, the same steps have been done but mixing the two salts which are cobalt nitrate and yttrium nitrate on magnetic stirrer for 1 h at 70 °C before adding PVA solution. Finally, these seed layers have been dried at 120 °C for a few minutes so as to get suitable adhesion of the seeded particles on the surface of the substrate. The main purpose of using seed layer is to supply nucleation sites by diluting the thermodynamic barrier between heterogeneous materials. Another advantage that has been observed is that when seed layer was used, the grown nanostructures were found to be well aligned, highly dense and uniform [13]. These seeded layers are thermal annealed at 210 °C for 1 h to vanish PVA, then annealed at 380 °C for 2 hour to improve crystallinity and remove hydroxide phase, now samples are being ready to the next step which is growth process.

To prepare growth solution, 0.1M cobalt nitrite (as a source of cobalt ions) and 0.1M Hexamine $C_6H_{12}N_4$ (as oxidized agent) are dissolved separately in distilled water and stirred for 10 min. Then, these two solutions are mixed and stirred for 10 min. For cobalt yttrium oxide preparation, the same procedure is done but before adding hexamine, yttrium nitrate (as a source of yttrium ions) is added to cobalt nitrate with appropriate amount and stirred together at 70°C for 1h to permit these two elements to well disperse, after 1h hexamine is added. The mixture was transferred into a Teflon-lined stainless steel autoclave where the substrates with seeded layers are vertically aligned inside the Teflon container. The autoclave was sealed quickly and maintained at 100°C for 4h in a digital temperature controlled oven. Then, the autoclave was cooled to room temperature naturally. The substrates are washed with distilled water to remove any residual solid particles from the surface or unreacted atoms, then the samples are dried in oven at 100°C for 30 min. Annealing process will be done inside furnace at 500°C for 1h to convert hydroxide phase $Co(OH)_2$ into Co_3O_4 . After that, the films are ready to be characterized.

The structural properties are determined by X-ray diffraction (XRD- 6000 Labx, supplied by Shimadzu, X-ray source is Cu). Film morphology was analyzed by MIRA3 model – TE-SCAN, (Dey Petronic Co. Tehran, Iran) Field Emission Scanning Electron Microscope (FESEM). The optical absorption spectra were obtained using UV–VIS spectrophotometer "OPTIMA SP-3000" within the wavelength range of (190-1100) nm.

3. Results and discussion

3.1 Structural properties (XRD)

X-ray diffraction patterns of synthesized cobalt oxide and cobalt yttrium oxide grown onto silicon substrates are shown in Fig. 1. It can be noticed that the patterns exhibit diffraction peaks around ($2\theta \sim 31.5044^\circ, 37.0796^\circ, 38.8496^\circ, 44.9558^\circ, 56.0177^\circ, 59.6460^\circ$ and 65.3097°) referred to

(202), (311), (222), (400), (422), (333) and (404) favorite directions respectively for cobalt oxide which is in agreement with (ASTM) card number 96-900-5888.

In addition to these peaks it can be noticed that the patterns exhibit diffraction peaks around ($2\theta \sim 33.8230^\circ$, 48.7611° and 57.8200°) referred to (400), (440) and (622) favorite directions respectively for yttrium oxide as shown in Table 1, which is in agreement with (ASTM) card number 96-100-9018 which proves the cubic structure for hydrothermally prepared cobalt oxide and illustrates the presence of Co_3O_4 phase and same beaks appeared with the researchers [14,15] and [16].

Crystallite size is estimated by Scherer's formula equation [16]:

$$D = \frac{K\lambda}{\beta \cos\theta} \quad (1)$$

where K is the shape factor (0.94), λ is 0.15405 nm which is the wavelength of the x-ray source, β is the full width at half-maximum (FWHM) and θ is the angle of the diffraction peak [14]. The average crystallite size D is 12.6 nm for cobalt oxide and it is 11 nm for cobalt yttrium oxide that means the size decreases with adding yttrium.

Lattice constant a is calculated by using the predominated orientation (311) from the following equation [14]:

$$d_{hkl} = \frac{a}{\sqrt{h^2 + k^2 + l^2}} \quad (2)$$

where hkl are miller indices and d_{hkl} is interplaner spacing which is calculated using Bragg law

$$n\lambda = 2 d_{hkl} \sin\theta \quad (3)$$

The calculated lattice constant of cobalt oxide nanostructure grown on silicon was 8.0348 Å and it was 7.998 Å for cobalt yttrium oxide nanostructure. Strain is calculated using the following relations [17] and [18]:

$$s = \frac{a - a_0}{a_0} \times 100\% \quad (4)$$

where a_0 is the standard lattice constant for unstained cobalt oxide lattice which equals 8.084 Å. The values of strain are -0.00609 and -0.01064 for cobalt oxide and cobalt yttrium oxide respectively. The negative value for strain is related to the compressive strain which is due to the nanosize effect.

Table 1 displays structural parameters calculated from XRD spectra for cobalt oxide and cobalt yttrium oxide. The addition of yttrium causes deformation or distortion to Co_3O_4 lattice, this may be due to large ionic radius of Y^{+3} which equals 0.9 Å compared with that of Co^{+3} which is 0.63 Å [19].

3.2 SEM analysis for thin films

SEM measurements were used to analyze the grain size and surface morphological of the seeded layers which prepared using spin coating technique and grown layer which prepared by hydrothermal method for Co_3O_4 and cobalt yttrium oxide thin films. The seed layer and growth film of pure Co_3O_4 nanoparticle showed the sphere like nanostructure which is in agreement with [14] as shown in Figs. 2a and 2b. The addition of yttrium to Co_3O_4 influence the surface morphology of sample, the structure changed to nanoflower which is observed to have been deteriorations, the seed layer is illustrated in figure 2c and growth film is shown in figures 2d and 2e at different magnifications. So, there is lattice deformation upon yttrium addition.

3.3 Optical properties

UV visible absorbance spectra of Co_3O_4 and cobalt yttrium oxide thin films in the range (200-1100) nm has been investigated as in Figure (3). The shoulder or peak position reflects the band gap of the nanoparticles, the peak of the spectra corresponds to the fundamental absorption edges in the sample [20]. It can be depicted two regions of optical transitions which is in agreement with [21]. Also, there is blue shift in absorption edges toward low wavelengths with yttrium addition which it may be related to the size decreasing of particles and attributed to the quantum confinement limit reaching of nanoparticles.

Also, the absorbance intensity decreases which may be due to the distortion in the crystal structure and SEM images show that the structure converted from nanospheres to nanoflowers which have high transmittance than that for nanospheres upon the addition of yttrium.

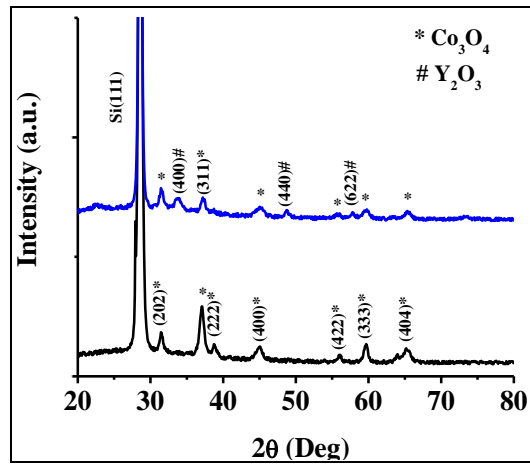


Fig. 1. XRD patterns of cobalt oxide and cobalt yttrium oxide grown onto Si substrates.

Table 1. Structure Parameters for Co_3O_4 and cobalt yttrium oxide.

Sample	2θ (Deg)	β (Deg)	d_{hkl} Exp.(Å)	D (nm)	hkl	d_{hkl} Std.(Å)	Phase	Card No.
cobalt oxide	31.5044	0.4779	2.8374	17.3	(202)	2.8589	Co_3O_4	96-900-5888
	37.0796	0.7168	2.4226	11.7	(311)	2.4375	Co_3O_4	96-900-5888
	38.8496	0.6371	2.3162	13.2	(222)	2.3349	Co_3O_4	96-900-5888
	44.9558	1.0354	2.0148	8.3	(400)	2.0219	Co_3O_4	96-900-5888
	56.0177	0.6372	1.6403	14.1	(422)	1.6498	Co_3O_4	96-900-5888
	59.6460	0.6372	1.5489	14.4	(333)	1.5550	Co_3O_4	96-900-5888
	65.3097	1.0354	1.4276	9.1	(404)	1.4286	Co_3O_4	96-900-5888
cobalt yttrium oxide	31.5044	0.6195	2.8374	13.3	(202)	2.8589	Co_3O_4	96-900-5888
	33.8230	0.9734	2.6480	8.5	(400)	2.6434	Y_2O_3	96-100-9018
	37.2566	0.6320	2.4115	13.3	(311)	2.4375	Co_3O_4	96-900-5888
	38.7611	0.5310	2.3213	15.9	(222)	2.3349	Co_3O_4	96-900-5888
	45.0442	1.1504	2.0110	7.5	(400)	2.0219	Co_3O_4	96-900-5888
	48.7611	0.7079	1.8661	12.3	(440)	1.8681	Y_2O_3	96-100-9018
	55.7522	1.0620	1.6475	8.5	(422)	1.6498	Co_3O_4	96-900-5888
	57.8200	0.8000	1.5934	11.3	(622)	1.5939	Y_2O_3	96-100-9018
	59.6460	1.0620	1.5489	8.6	(333)	1.5550	Co_3O_4	96-900-5888
	65.3982	0.8850	1.4259	10.7	(404)	1.4286	Co_3O_4	96-900-5888

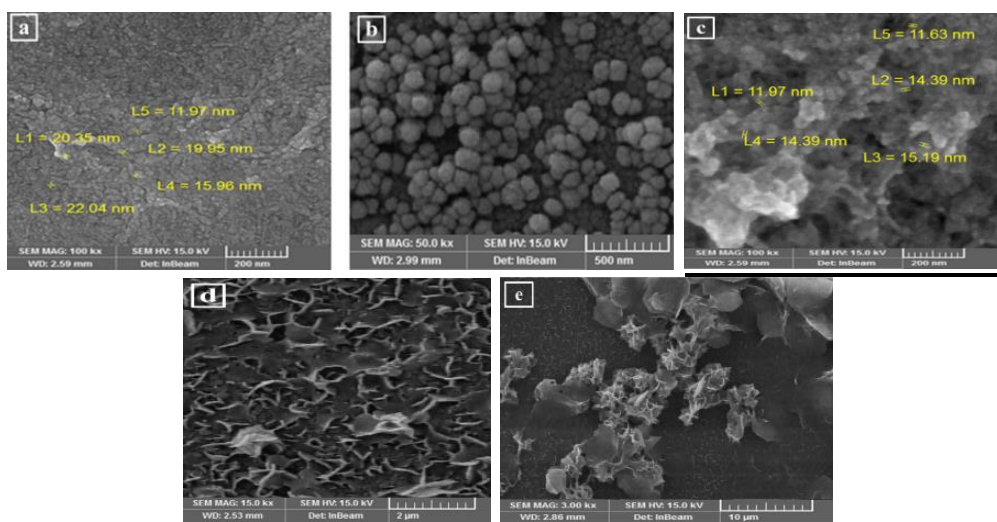


Fig. 2. SEM images of Co_3O_4 nanoparticles: a) seed layer, b) growth layer; for cobalt yttrium oxide: c) seed layer, d and e) growth layer with different magnifications.

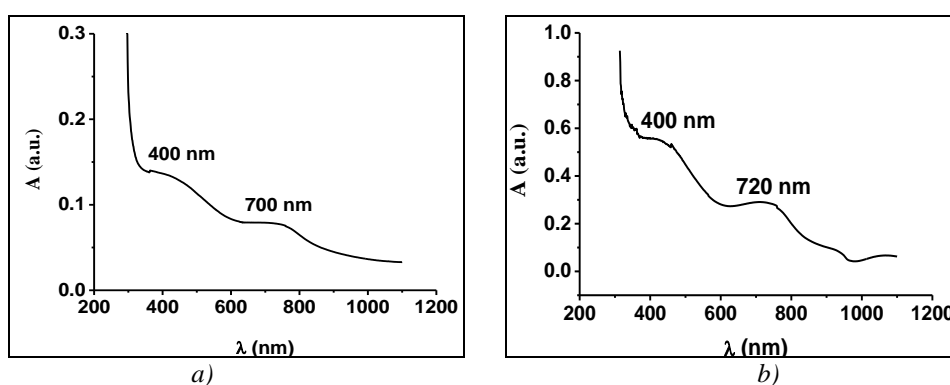


Fig. 3. UV-Vis absorption spectra of (a) Co_3O_4 and (b) cobalt yttrium oxide.

To estimate the value of the direct band gap from the above absorption spectra one can use Tauc relation [22,23]:

$$(\alpha h\nu)^n = B(h\nu - E_g) \quad (5)$$

where $h\nu$ is the photon energy in eV, α is the absorption coefficient in cm^{-1} , B is a constant related to the material, while the value of n is 2 for direct transitions, as in Co_3O_4 has a direct allowed band gap as mentioned by [1,2] and [15]. The band gap energy is obtained by extrapolating the linear part of the $(\alpha h\nu)^2$ versus photon energy ($h\nu$) on the axis $(\alpha h\nu)^2=0$ as shown in Fig. 4.

The optical absorption studies show that there are two direct band gaps in Co_3O_4 , the main energy band gap and a sub-band located inside the main energy gap, the values of these energy band gaps were determined to be 2.65 and 2 eV, respectively, which suffer from blue shift with respect to bulk Co_3O_4 . The corresponding values for the band gaps in the bulk are reported to be 2.13 and 1.52 eV [24]. The observed blue shift in the band gap was explained as originating in the finite size effects of the nanoparticles. For energy gap of cobalt yttrium oxide, blue shift happened, i.e. the optical energy gap increases with respect to Co_3O_4 with values 3.7 and 2 eV, this an indication that a strong quantum confinement happened and the particle size decreased.

Two direct optical band gaps are observed attributed to the excitations emanating from the presence of Co in two valence states +2 and +3 respectively. The Co^{3+} d states form a small sub-band within the main band gap whereas the Co^{2+} d states lie almost at the edge of the conduction band, while the valence band has a primarily O $2p$ character [25].

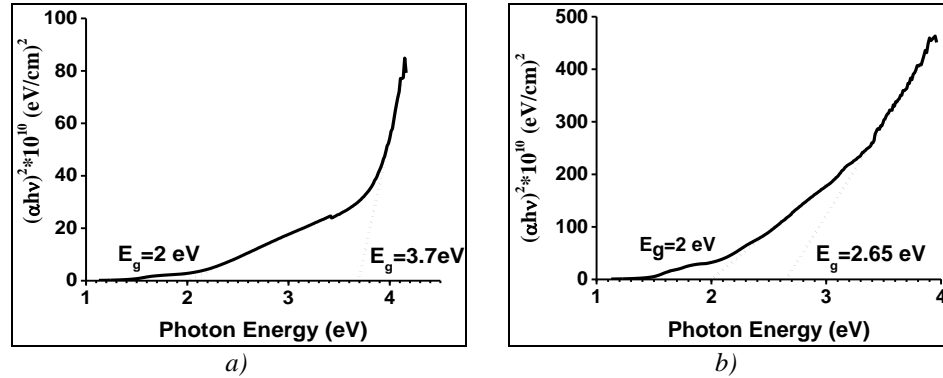


Fig. 4. Tauc plot of (a) Co_3O_4 and (b) Co-Y-oxide .

3.4 Current -Voltage (I-V) characteristics

I-V curve of photoconductive detector was measured in dark and under illumination. Fig. 5(a) and (b) illustrated the typical current –voltage properties of Co_3O_4 and Co-Y-oxide nanostructures, respectively. The measurement has been done under light with different intensities and the photocurrent increases with increasing light intensity. The measurements have been done with sweep voltage from -1V to 1V.

The forward dark current is generated due to the flow of majority carriers and the applied voltage injects majority carriers which cause to decrease of the built-in potential, as well as the width of the depletion layer. As the majority and minority carrier concentration is higher than the intrinsic carrier concentration ($n_i^2 < n_p$) which generate the recombination current at the low voltage region (0-0.35) Volt. This is because the excitation of electrons from valence band (V.B) to conduction band (C.B) will recombine with the holes which are found at the V.B., and this is observed by the little increase in recombination current at low voltage region.

After that there is a fast exponential increase in the current magnitude with increasing of the voltage and this is called diffusion current, which dominates [26]. While the value of the reverse bias current decreases with yttrium addition which is attributed to evolving defects and dislocations that have an effect on the mobility of charge carriers. Also these defects evolutions allow energy levels to be within the energy gap, these defects may act as active recombination centers, and consequently they decrease current flow across the junction. Figure 5a proves the Schottky behavior of the junction for Co_3O_4 but for Co-Y-oxide the ohmic contact predominates.

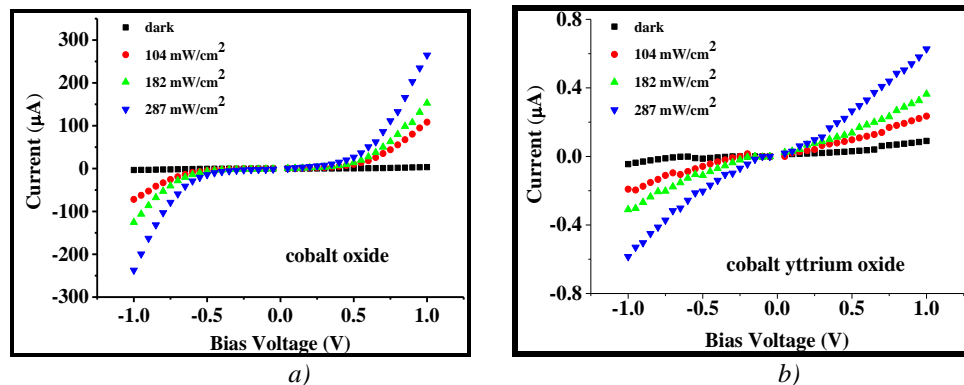


Fig. 5. I-V characteristics in the dark and under illumination for (a) Co_3O_4 and (b) Co.Y-oxide .

3.5 Responsivity R_λ

Spectral Responsivity R_λ is a performance parameter, defined as the photocurrent generated per unit of power of the incident light intensity on effective areas. The magnitude of the electrical signal output from a photoconductive detector is in response to a particular light power. The responsivity of a photoconductive detector is usually expressed in units of either amperes per watt or volts per watt of incident radiation power. To calculate the spectral responsivity of the tested detector (i.e., the responsivity as a function of wavelength), the photocurrent density generated from the tested detector is simply divided by the calculated power density as in the following equation [27]:

$$R_\lambda = J_{ph}(\lambda) / P_{in}(\lambda) \quad (6)$$

where $J_{ph}(\lambda)$ is the photocurrent density from the tested detector and $P_{in}(\lambda)$ is the incident power density measured with the photoconductive detectors as a function of wavelength. Fig. 6 show the responsivity R_λ of Co_3O_4 and Co-Y-oxide, the responsivity was high in visible region.

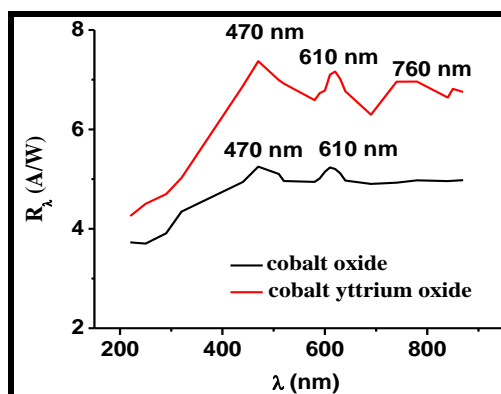


Fig. 6. The variation of spectral responsivity R_λ of Co_3O_4 and Co-Y-oxide.

3.6 Photo sensitivity

Conductivity increases when the light is turned on, and after the light is turned off, the current comeback to its original value. This process is repeated many time as shown in Figs. 7 and 8, and the rise time and fall time in this process are less than one second for each state turn (ON, OFF). The resistance-time (R-t) characteristics are taken with wavelengths (470 and 610) nm corresponding to maximum responsivity shown in Figs. 6 and 7. Also Table 2 shows the sensitivity for Co_3O_4 and Co-Y-oxide.

From results, the sensitivity increases with yttrium addition and this is attributed to the energy levels introduced by the addition atoms lying in the corresponding band gap of Co_3O_4 . Such states served as “hopping” states and increased the excitation probability of an electron to the conduction band. So, it becomes clear to be possible to control the response of the current in a semiconducting photodetector because the electrons in the nanoparticles receive their excitation energy from the power of the light source, it is possible to “switch” these nanoparticles reversibly between higher and lower states of conductivity. The results have been tabulated in Table 2.

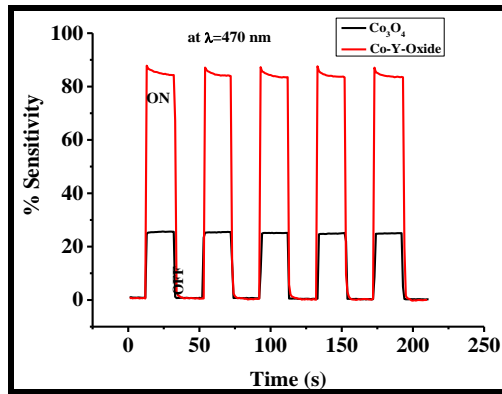


Fig. 7. Photo response time of the prepared Co_3O_4 and Co-Y-oxide photo sensor upon exposure to 470 nm light.

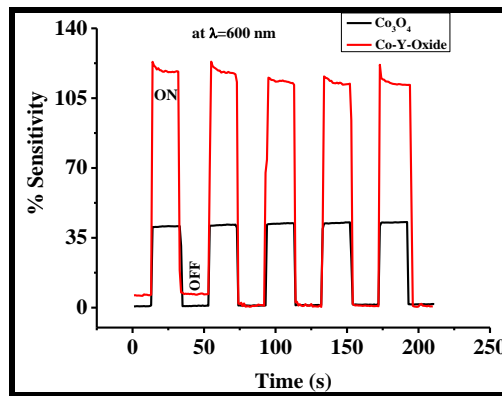


Fig. 8. Photo response time of the prepared Co_3O_4 and Co-Y-oxide photo sensor upon exposure to 610 nm light.

Table 2. Photo sensitivity as a function of wavelength for Co_3O_4 and Co-Y-oxide.

Sample	Sensitivity % at:	
	470nm	610 nm
Co_3O_4	39.7	40
Co-Y-oxide	84	111

4. Conclusions

Co_3O_4 and Co-Y-oxide nanostructures were successfully synthesized by hydrothermal method. SEM images of Co_3O_4 film show sphere shape like and Co-Y-oxide is observed to have nanoflower like. Optical energy gap is direct allowed. Photo conductive detector has been successfully fabricated from the prepared nano structure.

Two wavelengths which are near the two energy gaps have been used to examine our devices, higher sensitivity $\sim 111\%$ at 610 nm and very fast response time $< 1\text{sec}$ for Co-Y-oxide without any bias voltage, making them having potential applications as electrical gating for binary switching without necessary electric powder.

References

- [1] V. Patil, P. Joshi, M. Chougule, S. Sen, *Soft Nanoscience Letter* **2**, 1 (2012).
- [2] S. M. Jogade, D. S. Sutrave, V. B. Patil, *Int. Journal of Engineering Research and Application* **6**(9), 41(2016).
- [3] A. Osorio, A. V. Olmos, R. S. Berra, R. Escudero, *Rev. Adv. Mater. Sci.* **22**, 60 (2009).
- [4] F. Saeed, S. Jalil., Z. Parisa, *Journal of Nanostructure in Chemistry* **3**, 69 (2013).
- [5] X. Zhu, K. Hou, C. Chen, W. Zhang, H. Sun, G. Zhang , Z. Gao, *High Performance Polymers* **27**(2), 207 (2015).
- [6] S.K. Mishra, R.K. Srivastava, S.G. Prakash, R.S. Yadav, A.C. Panday, *Opto–Electronics Rev.***18**, 467 (2010).
- [7] N. V. Joshi, *Photoconductivity: Art, Science, and Technology*, Marcel Dekker, New York, 1990.
- [8] B. Sayan , K. M. Sheo, S. Biswarup , C. Purushottam , *Materials Science in Semiconductor Processing* **24**, 200 (2014).
- [9] I. M. Ali, R. M. Al-Haddad, K. T. Al-Rasoul, N. M. Ahmed, *Int. J. Adv. Res. in Sci., Eng. and Tech.* **1**(4), (2014).
- [10] J. B. Law, J. T. Thong, *Appl. Phys. Lett.* **88**, 133114 (2006).
- [11] C. S. Lao, J. Liu, Z. L. Wang, *Nano Letters* **6**(2), 263 (2006).
- [12] D. A. Kumar, F. P. Xavier, J. M. Shyla, *Archives of Appl. Sci. Res.***4**(5), 2174 (2012).
- [13] A. Zainelabdin, S. Zaman, G. Amin, O. Nur, M. Willander, *Crystal Growth & Design* **10**, 3250 (2010).
- [14] M. Manickam, V. Ponnuswamy, C. Sankar, R. Suresh, R. Mariappan, J. Chandrasekaran, *Int. J. Thin. Fil. Sci. Tec.* **5**(3), 155 (2016).
- [15] K. F. Wadekar, K. R. Nemade, S. A. Waghuley, *Research Journal of Chemical science* **7**(1), 2017.
- [16] S. Kerli, *Journal of the Korean Physical Society* **71**(7), 404 (2017).
- [17] J. Hassan, M. Mahdi, A. Ramizy, H. A. Hassan, Z. Hassan, *Superlattices and Microstructures* **53**, 31 (2013).
- [18] S. M. Mohammad, Z. Hassan, N. M. Ahmed, N. Al-Hardan, M. Bououdina, *Journal of Materials Science, Materials in Electronics* **26**, 1322 (2015).
- [19] Y. L. Hai-Jin, Z. Qing Li Yong, Liu Hou-Tong, *Chin. Phys. B* **22**(5), 057201 (2013).
- [20] I. M. Ali, R. M. Al-Haddad, K. T. Al-Rasoul, *Engineering & Technology* **1**(10), 2348 (2014).
- [21] V. R. Shinde, S. B. Mahadik, T. P. Gujar, C. D. Lokhande, *Applied Surface Science* **252**, 7487 (2006).
- [22] R. K. Willardson, A. C. Beer, *Semiconductor and Semimetals: Optical Properties of III-V Compounds*, Academic Press, New York 1996.
- [23] A. K. Sarfraz, S. K. Hasanain, *Acta Physica Polonica A* **125**(1), 139 (2014).
- [24] A. Gulino, P. Dapporto, P. Rossi, I. Fragala, *Chem. Mater.* **15**, 3748 (2003).
- [25] S. Thota, A. Kumar, J. Kumar, *Mater. Sci. Eng.* **B164**, 30 (2009).
- [26] A. Green, *Solar Cells*, translated by Y. Hassan, University of Mosul, p. 2817, 1989.
- [27] J. M. Lui, *Photonic Devices*, Cambridge University Press: Cambridge, 2005.